Petroleum Science 22 (2025) 5189–5202

Contents lists available at ScienceDirect

Petroleum Science

journal homepage: www.keaipublishing.com/en/journals/petroleum-science

Original Paper

Preparation and performance evaluation of a sand inhibiting and water control agent based on supramolecular interactions

Tian-Meng Lei [a,b,c,d], Ye-Fei Wang [a,b,c,*], Ming-Chen Ding [a,b,c], Wu-Hua Chen [a,b,c], Zhen-Ye Yu [a,b,c], Zhi-Xue Huang [a,b,c], Motorova Kseniya Alexandrovna [d,**]

[a] State Key Laboratory of Deep Oil and Gas, China University of Petroleum (East China), Qingdao, 266580, Shandong, China
[b] Key Laboratory of Unconventional Oil & Gas Development (China University of Petroleum (East China)), Ministry of Education, Qingdao, 266580, Shandong, China
[c] Shandong Key Laboratory of Oil and Gas Field Chemistry, School of Petroleum Engineering, China University of Petroleum (East China), Qingdao, 266580, Shandong, China
[d] Faculty of Geology, Lomonosov Moscow State University, Moscow, 119991, Russia

ARTICLE INFO

Article history:
Received 7 April 2025
Received in revised form
29 July 2025
Accepted 29 July 2025
Available online 5 August 2025

Edited by Yan-Hua Sun

Keywords:
Synergistic effect
Sand inhibition and water control
Theoretical simulation
Mechanism research

ABSTRACT

To address two key challenges (sand production and high water cut) in the development of loose sandstone reservoirs, a supramolecular sand inhibiting and water control agent, PDKM, was prepared using acrylamide (AM), methacryloxyethyltrimethyl ammonium chloride (DMC), styrene (SM), and γ-methacryloyloxypropyltrimethoxysilane (KH570) as monomers. The molecular structure and thermal stability of PDKM were confirmed by ^{1}H-NMR, FT-IR, and TGA. Compared with conventional agents containing only one or two functional monomers, PDM (AM/DMC) and PDSM (AM/DMC/SM), PDKM demonstrated superior sand inhibiting and water control performance due to the synergistic effects among its three functional monomers. PDKM forms a denser intermolecular network structure, resulting in a significantly lower average sand production rate (0.02 g/L) and a longer average sand breakthrough time (665 s), surpassing the "excellent" standard (≤ 0.05 g/L) specified in Q/SH 1020 2377-2020 for sand inhibitors. PDKM achieves a higher water–oil resistance ratio (6.47) and markedly reduces the produced fluid's water cut by 34.1%, greatly exceeding the "excellent" field criterion for water control agents (≥ 10% reduction). Theoretical simulation (DFT calculation) reveals strong intermolecular interactions, with PDKM–PDKM and PDKM–sand grain interaction energies of −0.065 and −0.085 Ha, providing a robust theoretical basis for its performance. These findings demonstrate that PDKM offers a promising and effective solution for the integrated control of sand production and water cut in loose sandstone reservoirs.

1. Introduction

The XX Oilfield in the Bohai loose sandstone reservoir is characterized by strong heterogeneity. The injected water preferentially flows through highly permeable channels during water injection, leading to early water breakthrough into production wells. This not only reduces capillary forces and weakens formation cementation strength but also results in a rapid increase in the water cut of produced fluids (Seright and Brattekas, 2021; Luo et al., 2022; Chen et al., 2023). In the mid-to-late stages of development, the elevated fluid shear forces caused by high flow rates can disrupt the structural integrity of the formation skeleton under high liquid production conditions. This phenomenon leads to significant sand production, compromising the formation's stability and causing substantial formation damage (Ross et al., 2006; Zhu et al., 2021; Duan et al., 2024). "Sand production" refers to the migration of sand grains from the reservoir into the wellbore along with the produced fluids during oil and gas production. Sand production is one of the most critical challenges in reservoir

* Corresponding author.
** Corresponding author.
E-mail addresses: wangyf@upc.edu.cn (Y.-F. Wang), motorova.ks@yandex.ru (M.K. Alexandrovna).

Peer review under the responsibility of China University of Petroleum (Beijing).

https://doi.org/10.1016/j.petsci.2025.07.022

development, as the produced sand can cause a variety of operational and environmental issues (Duan et al., 2024), including: (1) the corrosion and blockage of surface and downhole equipment, (2) subsidence of the formation rock and borehole wall instability, (3) permeability reduction in the oil layer, leading to decreased production efficiency and lower recovery factors, and (4) environmental pollution, posing safety and health hazards. Based on reservoir characteristics and economic feasibility, sand control techniques can be broadly categorized into mechanical sand control and chemical sand inhibition (Salehi et al., 2019; Duan et al., 2024). Mechanical sand control involves using tools, e.g., sieve tubes and slotted liners, during drilling and completion to physically block sand entry into the wellbore (Salehi et al., 2019; Duan et al., 2024). However, these methods do not address the root cause of sand production and have several limitations: complex and expensive equipment, potential damage to the wellbore, difficulty in achieving interlayer isolation, and limited effectiveness against fine sand particles (Salehi et al., 2019; Wu et al., 2024). In contrast, chemical sand inhibiting involves injecting chemical agents into the formation to enhance the strength of the interactions between sand grains, thereby transforming loose individual sand grains into more stable aggregates. This method strengthens the formation structure and suppresses sand production. It offers several advantages: the process is simple, no mechanical devices are left in the wellbore, remedial operations are straightforward, and it is cost-effective and efficient. As such, chemical inhibition can complement and outperform mechanical methods in controlling sand production at its source (Wu et al., 2024; Lei et al., 2025).

In addition, sand production often coincides with high water cut, which can reduce the effectiveness of water flooding and impede normal production (Lei et al., 2025). High water cut introduces additional issues such as pipeline erosion, reduced pump efficiency, and increased operational costs for oil–water separation and wastewater treatment (Qi et al., 2013). Similar to sand inhibiting, water control techniques can also be divided into mechanical and chemical approaches based on the mechanism of water production (Ahmed et al., 2020; Qin et al., 2020). Mechanical water control typically employs packers to isolate high water-producing zones, thereby preventing water from entering the wellbore and interfering with oil production from other layers. However, this approach has limitations: it is suitable only for reservoirs with a single water-producing layer and requires a stable interlayer of at least 1.5 m between the oil and water zones. Furthermore, construction conditions can be restrictive (Denney, 2001; Sun and Bai, 2017; Li Y.K. et al., 2019; Deng et al., 2021; Shu et al., 2023; Tian et al., 2023). Chemical water control involves injecting chemical agents into the water-bearing zones to interact with the formation and block high-permeability channels, thus achieving water control and oil stabilization. This method is advantageous because it is simple to implement, highly effective, reliable, and economical. It also addresses situations that mechanical methods cannot, such as layered water production with narrow interlayers or casing deformation that prevents effective zonal isolation (Denney, 2001; Sun and Bai, 2017; Li Y.K. et al., 2019; Deng et al., 2021; Shu et al., 2023; Tian et al., 2023). Therefore, it is necessary to apply chemical sand inhibiting and water control measures for the XX oilfield of Bohai loose sandstone reservoir.

Recent data indicate a steady increase in the annual implementation of sand inhibiting and water control operations in the XX oilfield of the Bohai loose sandstone reservoir. This trend not only leads to more frequent interventions in oil and water wells but also significantly increases production costs. Owing to the reliance on single-function treatment strategies, approximately 48% of oil wells experience sand production following water control operations. In comparison, 50% of wells treated for sand control suffer from high water cut issues (Lei et al., 2025). These statistics highlight a major limitation of conventional practices: the disjointed application of sand inhibiting and water control measures often results in poor coordination and fails to address the root causes of the problems. Therefore, it is urgent to develop and adopt integrated sand inhibiting and water control technologies that can simultaneously address both challenges in a single treatment (Lei et al., 2025).

In recent years, based on insights from field applications, the advanced concept of integrated sand inhibiting and water control technology has shifted toward enhancing the residual strength of the formation, thereby increasing the maximum sand-free rate (MSFR) and reducing the water cut-rather than merely improving consolidation strength (Alakbari et al., 2020; Li J.D. et al., 2022a). Guided by this concept, various sand inhibiting and water control agents have been developed, including cationic polymers, nanoparticles, polyacrylamide hydrogels, and zeta potential changers (Alakbari et al., 2020; Li J.D. et al., 2022a). Although these control agents have shown promise in reducing both sand production and water cut to varying degrees, there remains a need to develop more effective formulations with improved performance and reliability. Among these, cationic polymers are particularly noteworthy due to their dual functionality. These polymers can adsorb onto sand grain surfaces via electrostatic interactions, forming a protective adsorption layer that mitigates the detachment of sand grains. Simultaneously, their polymer chains swell in water, narrowing pore channels and restricting water flow, while collapsing in oil, thereby preserving oil layer permeability (Marandi et al., 2018; Lei et al., 2025). Building on this foundation, we propose the strategic incorporation of hydrophobic monomers (promote hydrophobic association and enhance the strength of the intermolecular network) and monomers capable of forming hydrogen or hydroxyl bonds (facilitate adsorption bridging and promote self-aggregation) into the backbone of cationic polymers. Through these modifications and synergistic effects, we aim to construct supramolecular systems capable of improved sand grain agglomeration and enhanced overall performance in sand inhibiting and water control (Li X.Q. et al., 2017; Duan et al., 2024; Lei et al., 2025) (Fig. 1). “Supramolecular interaction” refers to assembling polymer chains into three-dimensional macromolecular networks through non-covalent interactions such as electrostatic forces, hydrogen bonding, π–π stacking, and coordination bonding. These interactions impart the system with superior adaptability, structural tunability, and responsiveness to environmental stimuli (Joseph et al., 2024; Huo et al., 2024; Rijns et al., 2024; Tang et al., 2024). In recent years, supramolecular polymers have attracted growing attention as promising functional agents. Leveraging supramolecular interactions to design these polymers holds significant application potential. This approach offers a practical pathway for elucidating the mechanisms underlying sand inhibiting and water control and serves as a strategic route for developing high-performance materials tailored for enhanced oil recovery (Joseph et al., 2024; Huo et al., 2024; Rijns et al., 2024; Tang et al., 2024).

This study was inspired by the remarkable adhesion ability of marine mussels, which adhere firmly to rocks and various underwater surfaces through the secretion of foot proteins characterized by excellent self-healing properties (Li L. et al., 2015a, 2015b, 2015c, 2022). Therefore, designed and synthesized a novel supramolecular sand inhibiting and water control agent PDKM by incorporating the cationic monomer methacryloxyethyltrimethyl ammonium chloride (DMC), hydrophobic monomer styrene (SM), and hydrogen-bonded monomer γ-methacryloyloxypropyltrimethoxysilane (KH570) into an acrylamide (AM) polymer backbone, serving as the primary structural framework (Li L. et al.,

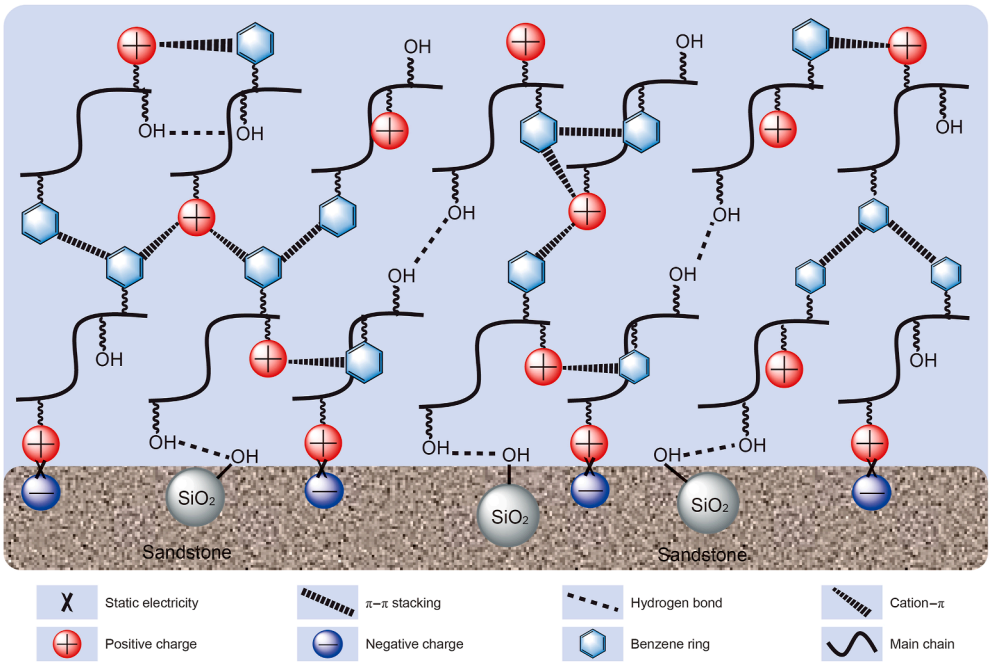

Fig. 1. Schematic diagram highlighting various supramolecular interactions.

2015c, 2024; Li X.Q. et al., 2017). In this work, we systematically investigated the structure–activity relationship and underlying mechanism of the sand inhibiting and water control agent PDKM, with a particular focus on the synergistic interactions among its functional monomers. The objective was to deepen the theoretical understanding of integrated sand inhibiting and water control processes and provide a more rational and scientifically grounded approach for designing and developing next-generation functional agents in this domain.

2. Experimental materials, instruments, and procedures

2.1. Experimental materials

The main chemicals employed in the study include: AM (≥ 98.0%), DMC (≥ 99.0%), SM (≥ 99.0%), KH570 (≥ 99.0%), ferrous sulfate ($FeSO_4{\cdot}7H_2O$, ≥ 99.5%), hydrogen peroxide (H_2O_2, ≥ 99.5%), 2, 2′-azobis(2-methylpropionamidine) dihydrochloride (V50, ≥ 99.5%), sodium hydroxide (Na OH, ≥ 99.7%), calcium chloride ($CaCl_2$, ≥ 99.7%), magnesium chloride ($MgCl_2$, ≥ 99.7%), sodium sulfate (Na_2SO_4, ≥ 99.7%), sodium bicarbonate ($NaHCO_3$, ≥ 99.7%), potassium chloride (KCl, ≥ 99.7%), sodium chloride (NaCl, ≥ 99.7%), alkaline alumina, neutral alumina (Al_2O_3, ≥ 99.5%), quartz sand (0.120–0.180 mm; 0.380–0.830 mm), and kaolin (0.050–0.071 mm).

The crude oil used in the experiments was obtained from the XX block of the Bohai Oilfield and exhibited a viscosity of 47.6 mPa·s at 65 °C and a shear rate of 7.34 s^{-1}.

2.2. Preparation of agents

To remove the polymerization inhibitors, the DMC, SM, and KH570 were purified by passing through chromatography columns packed with alumina. The monomers, AM, DMC, SM, and KH570, were then accurately weighed, dissolved in 120 mL of deionized water, and stirred until uniformly dispersed (by adding 0.1% sodium dodecyl sulfate, SDS). The pH of the mixed system was then adjusted to 7 using a sodium hydroxide solution. The reaction mixture was transferred into a three-necked flask and deoxygenated for 30 min using nitrogen. It was then cooled to 5–10 °C using an ice-water bath. The polymerization reaction was initiated by adding a certain amount of initiator (H_2O_2/$FeSO_4{\cdot}7H_2O$, V50). The mixture was kept at a low temperature for 6 h and subsequently heated to 55 °C for an additional 2 h. The resulting gel was prepared into a solution and dialyzed against deionized water for 3 days. It was then freeze-dried (−50 °C) to yield a white powder, the final product, PDKM (wherein the ratios M_{AM}: M_{DMC}: M_{SM}: M_{KH570} corresponded to 47: 47: 5.67: 0.33, M is the amount of substance). The total mass fraction (AM/DMC/SM/KH570) of the reaction monomer was maintained at 60% throughout the process. PDSM (M_{AM}: M_{DMC}: M_{SM} = 47: 47: 6) and PDM (M_{AM}:M_{DMC} = 50: 50) were also synthesized using the same method (Lei et al., 2025). The synthetic routes are shown in Fig. 2.

It is worth noting that the primary raw materials for PDKM synthesis, acrylamide (AM) and methacryloxyethyltrimethyl ammonium chloride (DMC), are both inexpensive and widely available industrial chemicals. In contrast, the functional monomers styrene (SM) and γ-methacryloyloxypropyltrimethoxysilane (KH570) are expensive, but they are only used in very small, controlled amounts (~6% of the total monomer molar ratio). The overall cost has remained within a controllable range. Additionally, the supramolecular sand inhibiting and water control agent PDKM is non-toxic and harmless to the environment, with no irritating odors released during storage or application.

2.3. Structure characterization and performance evaluation

2.3.1. Chemical structure characterization

The ^{1}H-NMR spectra of the PDM, PDSM, and PDKM agents were recorded using D_2O as a solvent (using an AVANCE NEO 600M instrument). Their FT-IR spectra were also recorded (using an IFS 125HR spectrometer), and samples were also subjected to thermogravimetric analysis (TGA) (using a THERMOSTEP analyzer).

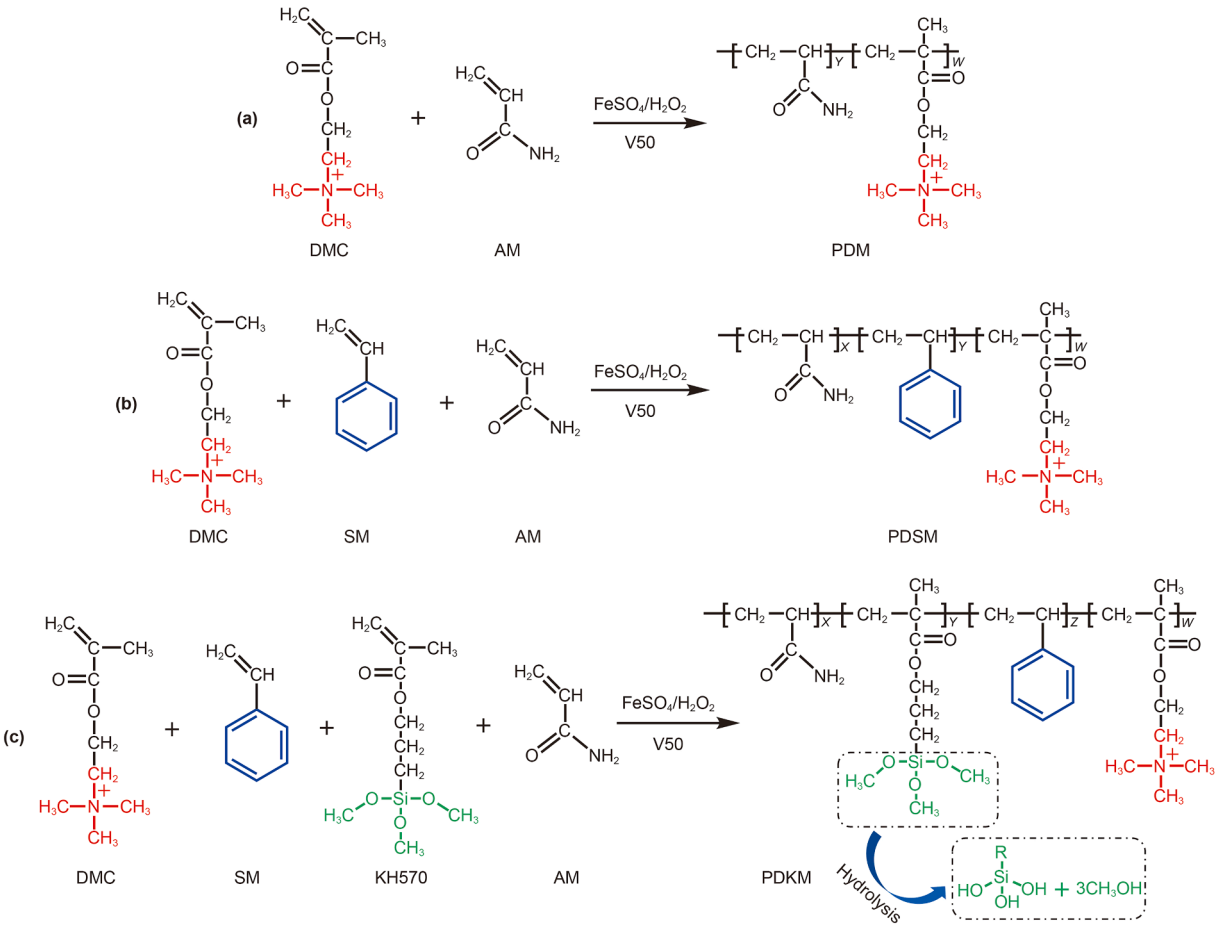

Fig. 2. Synthesis of the supramolecular sand inhibiting and water control agents.

2.3.2. Basic performance evaluation

2.3.2.1. Critical association concentration. The viscosities of solutions of the supramolecular sand inhibiting and water control agents were measured using a Brookfield viscometer (at 65 °C and 7.34 s^{-1}). The procedure followed the Chinese Petroleum Industry Standard (SY/T 5862-2020). The composition of the simulated water used to prepare the solutions is provided in Table 1.

A scanning electron microscope (SEM; model JSM-IT810) was also used to observe the microstructures of the supramolecular sand inhibiting and water control agents in solution (prepared at a concentration of 1000 mg/L using deionized water).

2.3.2.2. Static adsorption. Solutions of the supramolecular sand inhibiting and water control agents were first prepared at concentrations of 5, 10, 15, 20, 40, 60, and 100 mg/L using simulated water. The absorbances of these solutions (using the simulated water as reference sample) were then measured at 202.2 nm using a UV–visible spectrophotometer (model UV-3100PC). The absorbance data were then plotted and least-squares fitted to produce standard absorption curves.

Absorption experiments were then carried out. (1) 20.0 g of quartz sand (0.120–0.180 mm) was mixed with sand inhibiting and water control agent solutions (100.0 g) in conical flasks (150 mL) and aged for 24 h in an oven (at 65 °C) to reach equilibrium, with intermittent shaking every hour to ensure adequate contact between phases. (2) Thereafter, the clear upper liquids were removed from the conical flasks and centrifuged (4000 r/min, 20 min). (3) The centrifuged solutions were then diluted to the concentration range of the standard curves and their absorbance measured at 202.2 nm using the UV–visible spectrophotometer. (4) The concentrations of the polymer solutions after reaching adsorption equilibrium were then calculated using the standard curve equations (Lei et al., 2025). Finally, we calculated the static adsorption capacity F (mg/g) of each agent using Eq. (1):

$$F = \frac{(C_0 - C)V}{m_s} \quad (1)$$

where C_0 is the concentration of the original polymer solution, mg/L; C is the concentration of polymer solution after reaching adsorption equilibrium, mg/L; V is the volume of the solution, L; and m_s is the mass of quartz sand, g.

Table 1
Composition of the simulated water used in the experiments.

Ion	$K^+ + Na^+$	Mg^{2+}	Ca^{2+}	Cl^-	SO_4^{2-}	HCO_3^{2-}	TDS
Concentration, mg/L	4856.5	594.5	134.0	8937.0	1283.0	87.0	15937.0

2.3.3. Sand inhibiting performance

2.3.3.1. Sand leakage time. The experimental evaluation of sand leakage time was conducted with reference to the Chinese Patent CN118329696A (*"A rapid method for evaluating the performance of sand inhibitor"*) implementation, and the experimental steps are as follows: (1) Weighed samples of quartz sand (75.0 g, 0.120–0.180 mm) and sand inhibiting and water control agent solution (100.0 g) were added to a separatory funnel (250 mL). The inlet and outlet of the funnel were closed. (2) The separatory funnel was then placed in an oven (65 °C) and aged for 2 h. (3) The time for the complete leakage of the sand grains was then determined (excluding the time for solution leakage).

2.3.3.2. Sand production rate. The experimental evaluation method refers to the Chinese Patent CN118275289A (*"A new method for evaluating polymer sand inhibitor suitable for large displacement production conditions in offshore oilfields"*), and the experimental steps are as follows: (1) Samples of quartz sand (0.380–0.830 mm) and kaolin (0.050–0.071 mm) were weighed in a mass ratio of 21.2:1.0, the components were evenly mixed and then transferred to a sand tube (⌀2.5 cm and 10 cm long). (2) The inlet and outlet of the sand tube were then covered with 150 mesh single-layer screens. (3) Simulated water (2.0 PV) was then injected into the sand tube in the forward direction at a rate of 1 mL/min, supramolecular sand inhibiting and water control agent solution (2.0 PV) was then injected into the sand tube in the reverse direction at a rate of 1 mL/min, the inlet and outlet of the sand tube were then sealed and the tube aged in an oven (65 °C) for 24 h. (4) Simulated water was then injected into the sand tube in the forward direction at a rate of 100 mL/min for 1 h, the effluent was collected and filtered using a pre-dried filter paper. (5) The filter paper was then dried in an oven at 105±2 °C for 2 h (note that the filter paper was dried in the same as previously used). The sand production rate Q (g/L) was calculated using Eq. (2):

$$Q = \frac{m_2 - m_1}{V} \tag{2}$$

where m_1 is the mass of the filter paper, g; m_2 is the mass of the filter paper and sand residue after filtration, g; and V is the volume of the filtrate, L.

Note: The experimental method described above (forward water flooding followed by reverse injection of supramolecular sand inhibiting and water control agent solution) simulates the actual field operation in the XX Bohai loose sandstone oilfield. More precisely, the process involves injecting sand inhibiting and water control agent solution via the production well, followed by a shut-in period. Water is then injected from the injection well to displace fluids and enhance production. Furthermore, the field single well liquid producing capacity was converted to an indoor experimental displacement rate of 100 mL/min.

2.3.4. Water control performance

2.3.4.1. Selective water control. (1) Two sand tubes S_1 and S_2, which were prepared with the same permeability (2000±50 mD), were saturated with simulated water and crude oil, respectively, and then aged for 72 h. (2) Simulated water and crude oil were then (forward) injected into S_1 and S_2 at a rate of 1 mL/min, respectively. The corresponding permeabilities K_w and K_o were measured during stable pressures. (3) Supramolecular sand inhibiting and water control solution (0.5 PV) was (reverse) injected into S_1 and S_2, respectively, and aged for 24 h. (4) Simulated water and crude oil were once again (forward) injected into S_1 and S_2, respectively, and the corresponding permeabilities K_w' and K_o' were measured during new stable pressures (the experimental temperature used was 65 °C). The measurement method references the standard in the Chinese Oil and Gas Industry (SY/T 6567-2016) with implementation. The residual resistance coefficient F_{RR} (dimensionless) and standard water-oil resistance ratio N_{FRR} (dimensionless) were calculated using Eqs. (3) and (4):

$$F_{RRS_1} = \frac{K_w}{K_w'}$$
$$F_{RRS_2} = \frac{K_o}{K_o'} \tag{3}$$

$$N_{FRR} = \frac{F_{RRS_1}}{F_{RRS_2}} \tag{4}$$

where K_w is the permeability when S_1 was injected with simulated water, D; K_o is the permeability when crude oil was injected into S_2, D; K_w' is the subsequent water-flooding permeability in S_1 after injection with supramolecular sand inhibiting and water control agent solution, D; K_o' is the subsequent oil-flooding permeability in S_2 after injection with supramolecular sand inhibiting and water control agent solution, D; F_{RRS_1} is the residual resistance coefficient of S_1 (water tube) after injection with supramolecular sand inhibiting and water control agent solution; and F_{RRS_2} is the residual resistance coefficient of S_2 (oil tube) after injection with supramolecular sand inhibiting and water control solution.

2.3.4.2. Water cut reduction. (1) Two sand tubes were prepared with permeabilities differing by a factor of 2 (2000±50 mD/4000 ±50 mD). (2) Both tubes were saturated with simulated water and their porosities and permeabilities were measured. (3) They were then saturated with crude oil, and the volume of oil used was recorded. The samples were aged for 72 h. (4) The two tubes were then connected in parallel to the displacement device and forward injected with simulated water until the produced water cut exceeded 95%. (5) 0.5 PV supramolecular agent solution was reverse-injected into both tubes, followed by 24 h of aging at 65 °C. (6) Simulated water was again injected in the forward direction at 1 mL/min and 65 °C until the water cut exceeded 95%. The experimental procedure references the Chinese Petroleum Industry Standard (SY/T 6567-2016) with implementation.

2.4. Theoretical simulations (DFT calculation)

DFT calculation was employed using the B3LYP functional to evaluate the intermolecular interaction energies. Grimme dispersion correction was introduced to improve energy accuracy. Meanwhile, a full-electron potential basis set was utilized to fully account for the influence of kernel electrons on valence electrons, thereby better describing intermolecular interactions. In addition, the DFT calculations are performed based on the 0 K conditions and yield pure electronic energies, which are independent of temperature. Although thermal effects such as vibrational contributions can influence total free energy at higher temperatures, their impact on solid/condensed phase systems is generally minimal at room temperature.

In this study, DFT calculations were used to investigate the interactions between the molecular structures of the synthesized agents and quartz sand surfaces. All calculations were performed using Gaussian 16 (Frisch et al., 2016). Geometric optimizations of all molecular models were first performed using B3LYP functionals combined with the def2SVP basis set. In addition, single-point energies were also calculated at the def2TZVP basis set level to obtain more reliable binding energies. The D3 dispersion correction was also introduced into the calculation process. All the

analyses and graphs presented in this work were generated using GaussView (Semichem, 2019), Multiwfn (v3.8dev) (Lu and Chen, 2021), and rendered using VMD (Humphrey et al., 1996). Interaction energies were calculated using the following formula:

$$E_{\text{int}} = E(\text{AB}) - E(\text{AB}) - E(\text{B}) \quad (5)$$

where E_{int} is the binding energy of the system; E(AB) is the energy of the total structure; and E(A) and E(B) are the energies of the individual components.

Also note that the active interaction sites were visualized by considering the electrostatic potential, and quartz sand was represented using a simplified $SiO(OH)_3$ structure to highlight the extremely strong negative charge on the sand's surface.

3. Results and discussion

3.1. Structure characterization

3.1.1. ^{1}H-NMR

Fig. 3 presents the ^{1}H-NMR spectra of three synthesized supramolecular sand inhibiting and water control agents. In Fig. 3, peak 1 (0.8–1.2 ppm), peak 2 (1.4–1.6 ppm), and peak 3 (1.9–2.1 ppm) are characteristic peaks corresponding to methyl, methylene, and methane groups, respectively. Similarly, peak 4 (3.0–3.2 ppm), peak 5 (3.3–3.4 ppm), and peak 6 (3.9–4.0 ppm) are associated with methyl groups on a quaternary ammonium group, methylene groups adjacent to a quaternary ammonium group, and methylene groups adjacent to an ester group, respectively. The large peak labeled as 7 (4.6–4.8 ppm) is caused by the solvent (D_2O). Finally, peak 8 (7.1–7.6 ppm) and peak 9 (3.5–3.7 ppm) are characteristic peaks associated with benzene rings and methyl groups connected to siloxanes, respectively. The presence of these characteristic peaks confirms that the KH570, SM, and DMC components were successfully grafted onto the polymer backbone during synthesis.

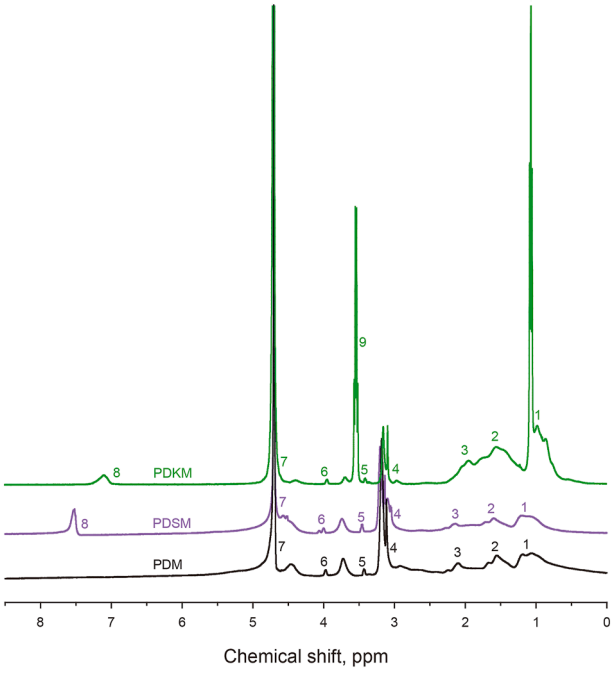

Fig. 3. ^{1}H-NMR spectra of the supramolecular sand inhibiting and water control agents.

3.1.2. FT-IR

Fig. 4 presents the FT-IR spectra of the three supramolecular sand inhibiting and water control agents. The key absorption bands are summarized as follows: a (700–710 cm^{-1}), b (760–770 cm^{-1}), c (870–880 cm^{-1}), and f (1450–1460 cm^{-1}) correspond to benzene rings; d (950–960 cm^{-1}) is a characteristic peak of quaternary ammonium groups; e (1030–1040 cm^{-1}) is a characteristic peak caused by Si–O–Si/Si–O–C moieties; g (1660–1670 cm^{-1}) and h (1720–1730 cm^{-1}) are peaks characteristic of C=O bonds in esters; and i (2930–2960 cm^{-1}), j (3170–3190 cm^{-1}), and k (3330–3360 cm^{-1}) are characteristic peaks corresponding to methyl, C=O bonds in amide groups, and NH_2 in amide groups. As Si–OH produces a characteristic peak near k. The higher intensity of the k peak from PDKM compared to PDM and PDSM confirms the successful grafting of KH570, SM, and DMC into the PDKM backbone (Chen et al., 2024; Xu et al., 2024). The copolymers were all target products.

3.1.3. TGA

Fig. 5 presents the TGA results of the three supramolecular sand inhibiting and water control agents. As the temperature was

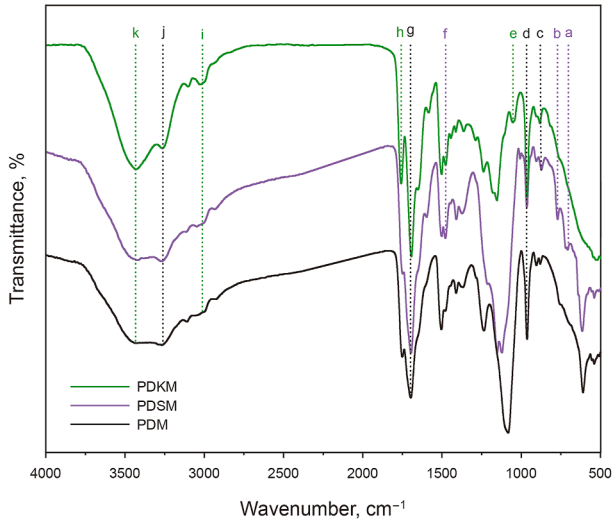

Fig. 4. FT-IR spectra of the supramolecular sand inhibiting and water control agents.

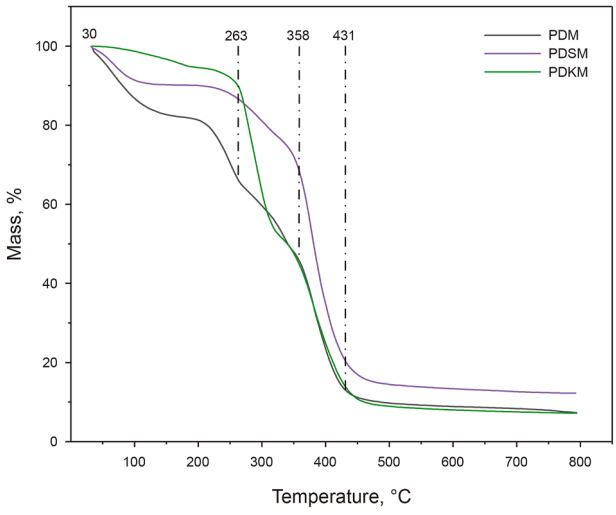

Fig. 5. TGA curves of the three supramolecular sand inhibiting and water control agents.

increased from 30 to 263 °C, the PDKM sample lost roughly 11% of its mass due to water evaporation and cleavage of amide groups. In contrast, the mass losses for PDSM and PDM were 14% and 35%, respectively. As the temperature was increased from 263 to 358 °C, progressive degradation of the polymer backbone occurred, with complete decomposition finishing around 431 °C. At this stage, the mass losses of the PDM, PDSM, and PDKM samples were approximately 87%, 80%, and 86%, respectively (Xu et al., 2024; Lei et al., 2025). It is worth noting that the thermal stability in the low-temperature range (30–263 °C) is more relevant for field application, as the reservoir temperature in the XX block of the Bohai loose sandstone oilfield is approximately 65 °C. Moreover, Fig. 5 shows that PDKM has better thermal stability compared to PDM and PDSM at this particular temperature.

3.2. Basic performance

3.2.1. Critical association concentration

To investigate the critical association concentration and injectivity of the supramolecular sand inhibiting and water control agents, the apparent viscosities of the agents were measured across a range of concentrations. When the actual concentration exceeds the critical association concentration, a three-dimensional network structure is formed within the solution, enhancing its sand inhibiting and water control performance. The results are shown in Fig. 6. The viscosity of the PDSM and PDKM solutions increases significantly when the solution concentration exceeds 2500 mg/L, indicating that the PDSM and PDKM agents have critical association concentrations (C^*) close to 2500 mg/L (Lei et al., 2024). When a solution has a concentration less than C^*, the molecules are relatively far apart, and the formation interactions are mainly intramolecular. Therefore, the viscosity of the solution increases slowly as the concentration increases. Once the solution concentration reaches C^*, the molecules are much closer and intermolecular interactions become dominant, resulting in the formation of large molecular aggregates and a sharp increase in viscosity (Lei et al., 2024). Fig. 6 also shows that the PDKM solution exhibits significantly higher viscosity than those of PDM and PDSM at the same concentrations. This enhanced viscosity behavior is attributed to three functional monomers (DMC, SM, and KH570), which enable a rich array of intermolecular forces, including hydrophobic association (π–π stacking), hydrogen bonding (hydroxyl bond), electrostatic interactions, cation–π, and π/cation–π. Under synergistic effects, these interactions contribute to the formation of a stronger spatial network structure with a larger hydrodynamic volume, leading to superior thickening capability (Li X.Q. et al., 2017; Li L. et al., 2015c, 2024; Lei et al., 2025). Note that the viscosity of the PDKM solution reaches around 55 mPa·s at a concentration of 5000 mg/L, indicating good injectability even at this relatively high concentration.

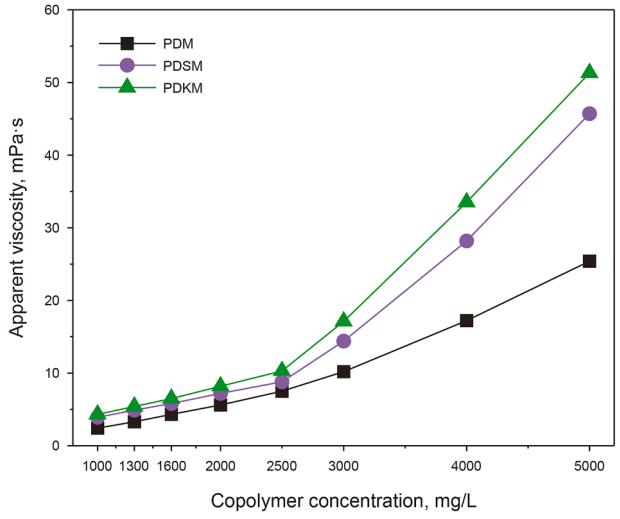

Fig. 6. Viscosity–concentration plots of the supramolecular sand inhibiting and water control agents.

To further elucidate the structural characteristics of the agents in solution, scanning electron microscopy (SEM) was used to observe the microscopic morphologies of the PDM, PDSM, and PDKM solutions, each prepared at 1000 mg/L in deionized water. The results are presented in Fig. 7. Compared to PDM and PDSM, PDKM forms a denser intermolecular network. The formation of macromolecular aggregates and more pronounced entanglement is clearly visible in the PDKM solution, consistent with the experimental results of apparent viscosity (Lei et al., 2024).

3.2.2. Static adsorption results

To better understand the static adsorption performance of the three supramolecular sand inhibiting and water control agents, we performed static adsorption experiments to determine the adsorption capacity of the agents on the surface of sand grains. In general, a greater adsorption capacity implies stronger agglomeration and bundling effects on sand grains (and vice versa). The UV absorbances of the supramolecular sand inhibiting and water control agents were first determined to establish the standard calibration curves shown in Fig. 8(a). After reaching adsorption equilibrium, the extracted solutions were diluted to $\leq$ 100 mg/L, and their concentrations were calculated using the calibration curves. Based on these values, isothermal adsorption curves were plotted for each agent, as presented in Fig. 8(b).

As shown in Fig. 8(b), the adsorption capacities of all three agents initially increase significantly with rising solution concentration. However, the rate of increase gradually decreases, and the curves plateau as adsorption approaches saturation. This observation indicates that at higher concentrations ($\geq$ 4000 mg/L), the available adsorption sites on sand surfaces become fully occupied, and further concentration increases yield minimal additional adsorption (Lei et al., 2025). Compared to PDM (8.7 mg/g) and PDSM (14.6 mg/g), the adsorption capacity of PDKM is the largest, at 16.3 mg/g. The superior performance of PDKM is attributed to the presence of quaternary ammonium groups, benzene rings, and silanol groups in its structure. These functional groups enable strong interactions between the polymer molecules and quartz sand, resulting in tighter and more stable adsorption (Li J.D. et al., 2022a; Li X.Q. et al., 2017; Li L. et al., 2015c, 2024).

3.3. Sand inhibiting performance

3.3.1. Sand leakage time

To rapidly assess the sand inhibiting performance of different functional polymers, we developed a method to evaluate the performance of sand inhibiting agents using sand leakage time (Chinese patent CN118329696A: *A rapid method for evaluating the performance of sand inhibitor*, which has demonstrated good correlation with the industry-recognized method (the sand inhibiting evaluation standard "Q/SH 1020 2377-2020"). In this method, a longer sand leakage time is positively correlated with a lower sand production rate, thereby serving as an effective indicator of sand inhibiting efficiency. Fig. 9 illustrates the sand leakage times for PDM, PDSM, and PDKM at various concentrations. As the concentration increases, the sand leakage time of the three supramolecular sand and control agents gradually increases. However, concentrations beyond 5000 mg/L led to no significant

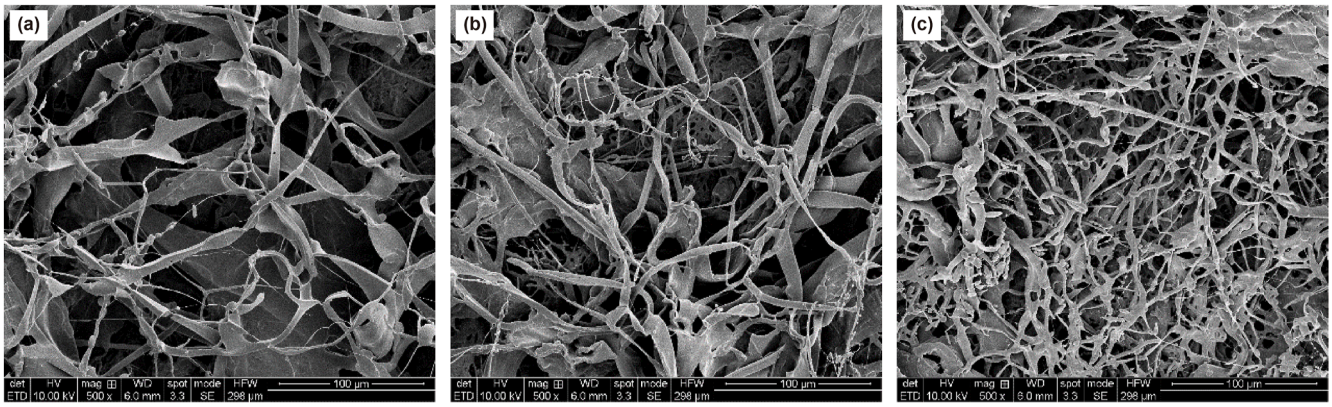

Fig. 7. SEM images of supramolecular sand inhibiting and water control agents in solution. (**a**) PDM; (**b**) PDSM; (**c**) PDKM.

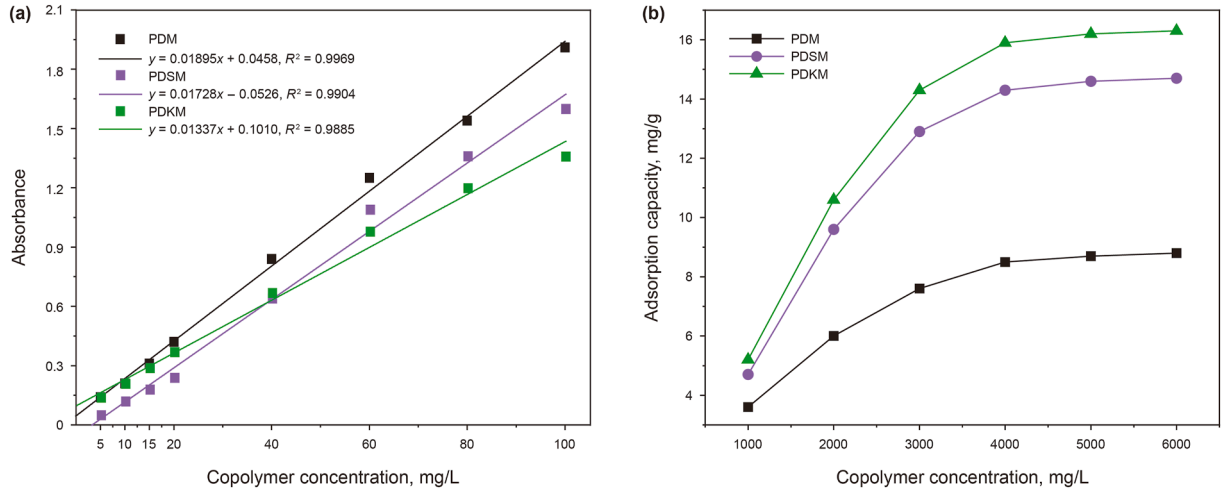

Fig. 8. (**a**) Standard absorbance curves of the three supramolecular sand inhibiting and water control agents. (**b**) Adsorption capacities of the agents at different concentrations.

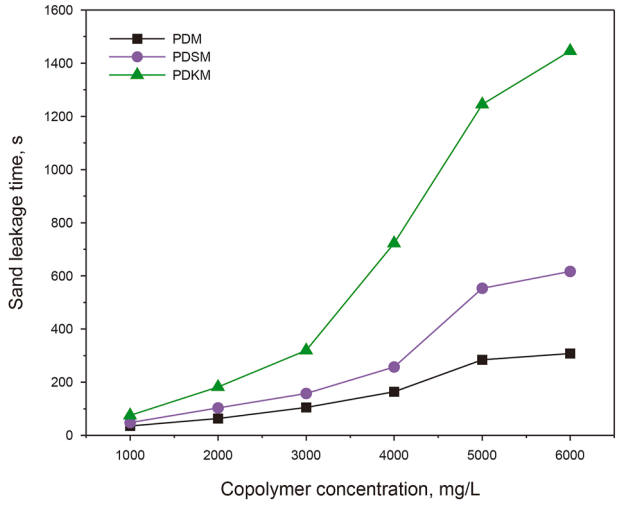

Fig. 9. Sand leakage time as a function of the concentration of supramolecular sand inhibiting and water control agents.

improvement in sand leakage time, consistent with the findings of adsorption saturation observed in static adsorption tests. The average sand leakage time of PDKM (665 s) is longer than both PDM (160 s) and PDSM (289 s). The superior performance of PDKM can be attributed to its incorporation of three functional monomers and the intermolecular synergistic effects (π–π stacking, hydrogen bond, electrostatic, cation–π, and π/cation–π), these interactions lead to stronger agglomeration and binding of sand grains, which effectively inhibits their vertical migration and prolongs the sand leakage time (Lei et al., 2025; Li X.Q. et al., 2017; Li J.D. et al., 2022b).

The adsorption of PDM, PDSM, and PDKM onto the sand grain surfaces was further investigated by observing the behavior of the adsorption film formation when sand and solution were mixed (Fig. 10). Quartz sand and solutions of the supramolecular sand inhibiting and water control agents were mixed and left to stand for 3–5 days. As shown in Fig. 10(a), the adsorption film/polymer concentration layer formed by PDKM (PDKM-1) is much thicker than those formed using PDM and PDSM (PDM-1 and PDSM-1, respectively). The dried sand agglomerates formed from these mixtures are then removed and observed, as shown in Fig. 10(b). The sand grain agglomerates formed by PDM (PDM-2) are relatively loosely aggregated with significant flocculent dispersions; those formed by PDSM (PDSM-2) have irregular, notched edges and some flocculent dispersions. PDKM (PDKM-2) forms more uniform, compact, and well-defined aggregates with minimal flocculent dispersion. To assess aggregate stability, the supernatants are decanted, and the remaining sand is manually stirred with a glass rod (Fig. 10(c)). The aggregates formed using PDKM

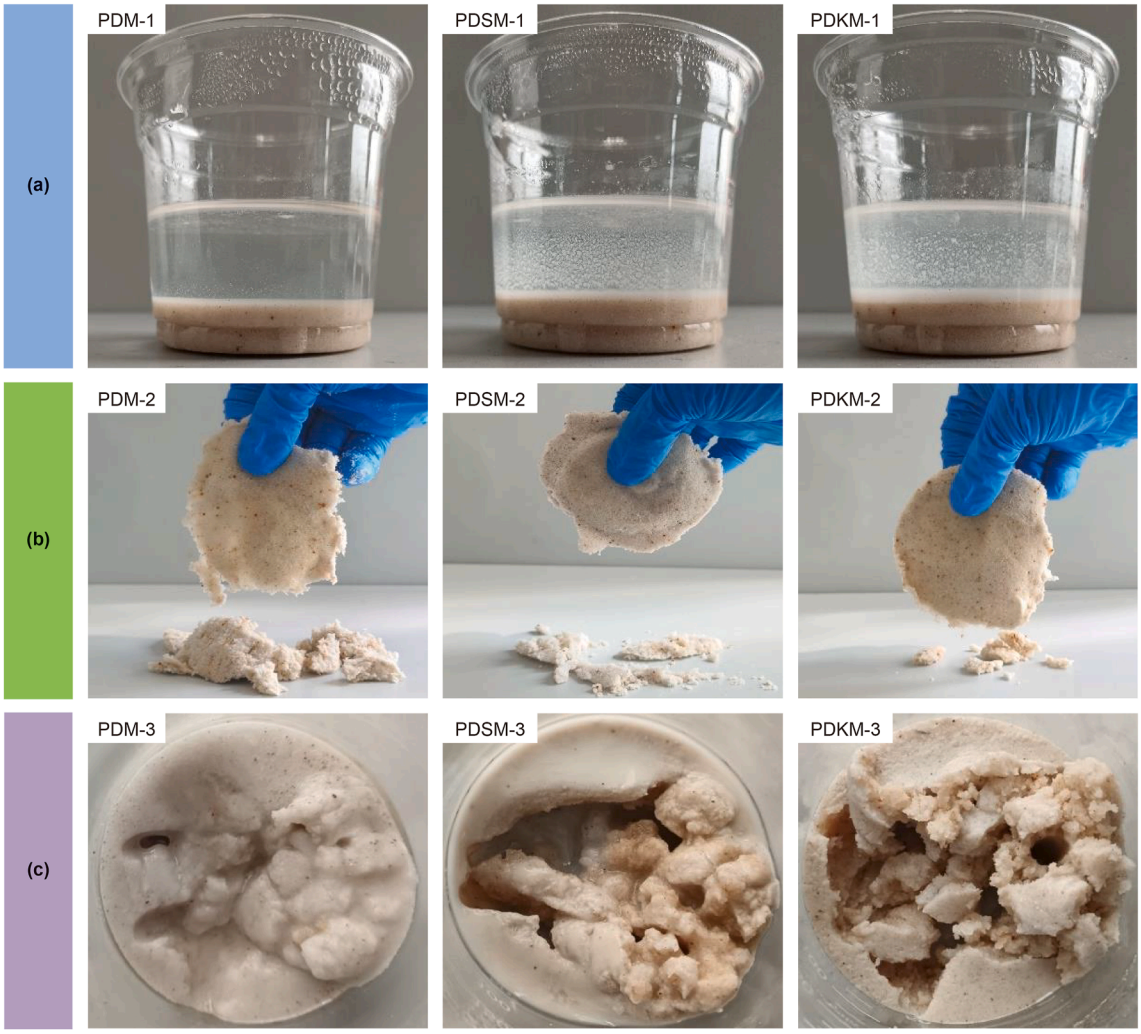

Fig. 10. (**a**) Adsorption film formation by the supramolecular sand inhibiting and water control agents on the sand grain surface. (**b**) Aggregation/bundling behavior of the sand grains. (**c**) Consolidation effect of sand grain agglomerates.

(PDKM-3) exhibited a better solid-like behavior (i.e. consolidation effect) and a better agglomeration/bundling effect with the sand grains compared to PDM-3 and PDSM-3. Therefore, PDKM has a better sand stabilization effect compared to the others.

3.3.2. Sand production rate

In industrial applications, a key metric for evaluating the performance of sand inhibiting agents is the sand production rate under specific conditions. According to enterprise standard Q/SH 1020 2377-2020 of the China Petrochemical Group Co., Ltd, we established a method that can effectively evaluate the performance of sand inhibiting agents at a flow rate of 100 mL/min (Chinese patent CN118275289A: "*A new method for evaluating polymer sand inhibitor suitable for large displacement production conditions in offshore oilfields*") and has been authorized. In addition, the method and the evaluation standard of sand inhibitor (Q/SH 1020 2377-2020) define "excellent" sand inhibiting performance if its sand production rate is $\leq$ 0.05 g/L. The lower the sand production rate, the more effective the sand inhibiting performance.

Fig. 11 presents the measured sand production rates of PDM, PDSM, and PDKM across concentrations ranging from 1000 to 6000 mg/L. The results show a general trend: the sand production

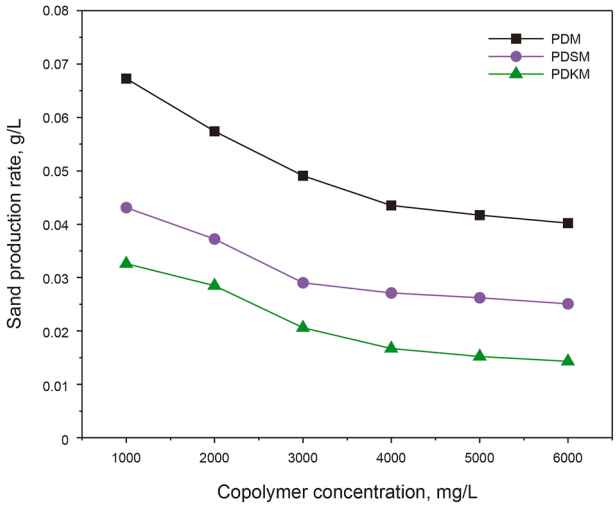

Fig. 11. Sand production rates of the supramolecular sand inhibiting and water control agents at different concentrations.

rate decreased with increasing concentration, eventually approaching a plateau. Specifically, the average sand production rates for the PDM and PDSM over the concentration range of 1000–6000 mg/L are 0.05 and 0.03 g/L, respectively. In contrast, the PDKM has an average sand production rate of 0.02 g/L, indicating a better sand inhibiting performance. The superior performance of PDKM is again attributed to its functional monomers, which allow the polymer to be more firmly adsorbed onto the sand grain surface (via π–π stacking, hydroxyl bond, electrostatic, cation–π, and π/cation–π interactions), these synergistic interactions result in a dense intermolecular network that binds tightly to sand grain surfaces, effectively aggregating them and resisting the mechanical erosion caused by high-velocity fluid flow (Lei et al., 2025; Li X.Q. et al., 2017; Li L. et al., 2015c, 2024).

3.4. Water control performance

3.4.1. Selective water control

The oil industry generally uses the standard water–oil resistance ratio (N_{FRR}) to evaluate the selective water control performance of water control agents. The larger the N_{FRR} value, the better the ability of the water control agent to block water preferentially over oil under the same conditions (effective water plugging without hindering oil production, thereby improving sweep efficiency). In this study, we evaluated the N_{FRR} values of the control agents at a concentration of 5000 mg/L, consistent with actual field application dosages. The results for the PDM, PDSM, and PDKM control agents are summarized in Table 2.

PDKM exhibits a significantly higher water–oil resistance ratio, outperforming PDM and PDSM by 125.8% and 28.0%, respectively, demonstrating that PDKM has superior selective water control capabilities. It more effectively reduces the permeability to water while maintaining permeability to oil, thus enabling selective flow regulation in porous media. This enhanced performance can be attributed to the synergistic effect of PDKM's three functional monomers. These monomers enable strong adsorption of the polymer onto pore surfaces. Additionally, polymer chain segments dispersed in the pore water phase act as 'adsorption anchors', which swell in water and shrink in oil. Consequently, PDKM creates higher resistance to water flow while allowing oil to pass and enhances water-blocking efficiency without adversely affecting oil mobility (Ye et al., 2010; Guo et al., 2014; Ahmed et al., 2023; Hayavi et al., 2023; Lei et al., 2025).

3.4.2. Water cut reduction

One of the most direct indicators of water control effectiveness in the field is the reduction in water cut of the produced fluid. A significant drop in water cut implies that oil production has increased, indicating the successful application of the water control agent. Because 5000 mg/L is the standard concentration used in field operations, this concentration was adopted in our laboratory experiments. The results of reduced water cut for PDM, PDSM, and PDKM are shown in Fig. 12. A noticeable reduction in water cut was observed during reverse injection of the sand inhibiting and water control agents, because the sand inhibiting and water control agents have selective water control effects. The agents can

Table 2
Resistance coefficients and residual resistance coefficients of supramolecular sand inhibiting and water control agents.

Agent	K_w	K_o	K'_w	K'_o	F_{RRS_1}	F_{RRS_2}	N_{FRR}
PDM	2.53	1.29	0.68	1.13	3.721	1.142	3.26
PDSM	2.48	1.34	0.38	1.15	6.526	1.165	5.60
PDKM	2.49	1.26	0.33	1.08	7.545	1.167	6.47

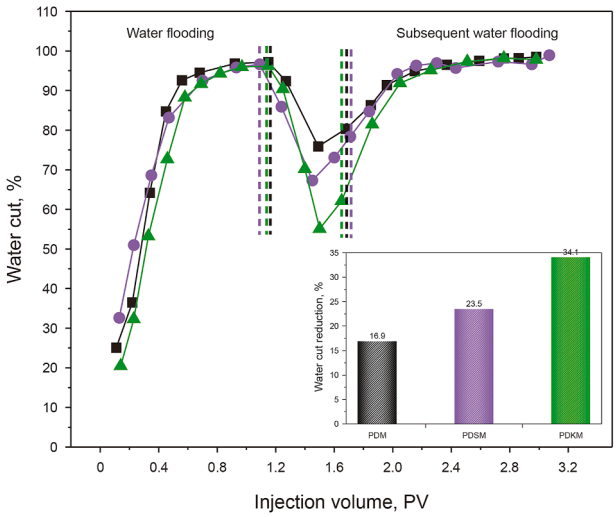

Fig. 12. Water cut reduction performance of various supramolecular sand inhibiting and water control agents.

reduce the permeability of the water layer without affecting the permeability of the oil layer. As a result, the agents prevent water channeling, redirect the injected fluids, and expand the sweep volume, lowering the water cut (Lei et al., 2024, 2025). The water cut values of PDM, PDSM, and PDKM are 16.9%, 23.5%, and 34.1%, respectively. PDKM outperformed the other agents, reducing the water cut by 101.8% more than PDM and 45.1% more than PDSM, confirming its superior water control performance. This improvement is again credited to the PDKM, which contains three functional monomers. The presence of PDKM allows for forming thicker and more stable adsorption layers on pore surfaces, along with a higher residual resistance coefficient in the aquifer. These effects reduce the permeability of high-permeability water-bearing zones without negatively impacting the permeability of the oil zones, thus expanding swept volume, enhancing oil displacement, and achieving the dual goals of water control and oil stabilization (Qiao and Zhu, 2010; Lai et al., 2013; Askarinezhad et al., 2021; Lei et al., 2025).

3.5. Mechanisms

3.5.1. Theoretical simulations

Theoretical simulations (DFT calculation) were performed to investigate the interactions (including intermolecular interactions) between the supramolecular sand inhibiting and water control agents and sand grains. Note that the molecular simulation calculations are facilitated using negatively charged SiO_2 to represent quartz sand. Fig. 13(a)–(c) shows the electrostatic potential maps of PDM, PDSM, and PDKM, respectively. In these images, the blue clouds represent regions of positive charge, with deeper blue indicating stronger positive electrostatic potential. Greater electrostatic potential leads to stronger attraction to the negatively charged quartz sand surface (Niu et al., 2025; Zhang et al., 2025). As shown in Fig. 13, the blue clouds in the PDKM are significantly deeper and more widespread than those in the PDM and PDSM, indicating a stronger affinity of PDKM for adsorption onto sand surfaces.

To further investigate the molecule-to-molecule and molecule-to-sand grain interactions, the interaction region indicator (IRI) function was used to visualize these interactions, as shown in Fig. 13(d)–(i). The corresponding adsorption energies were also calculated. In the IRI plots, the deeper the blue color, the stronger

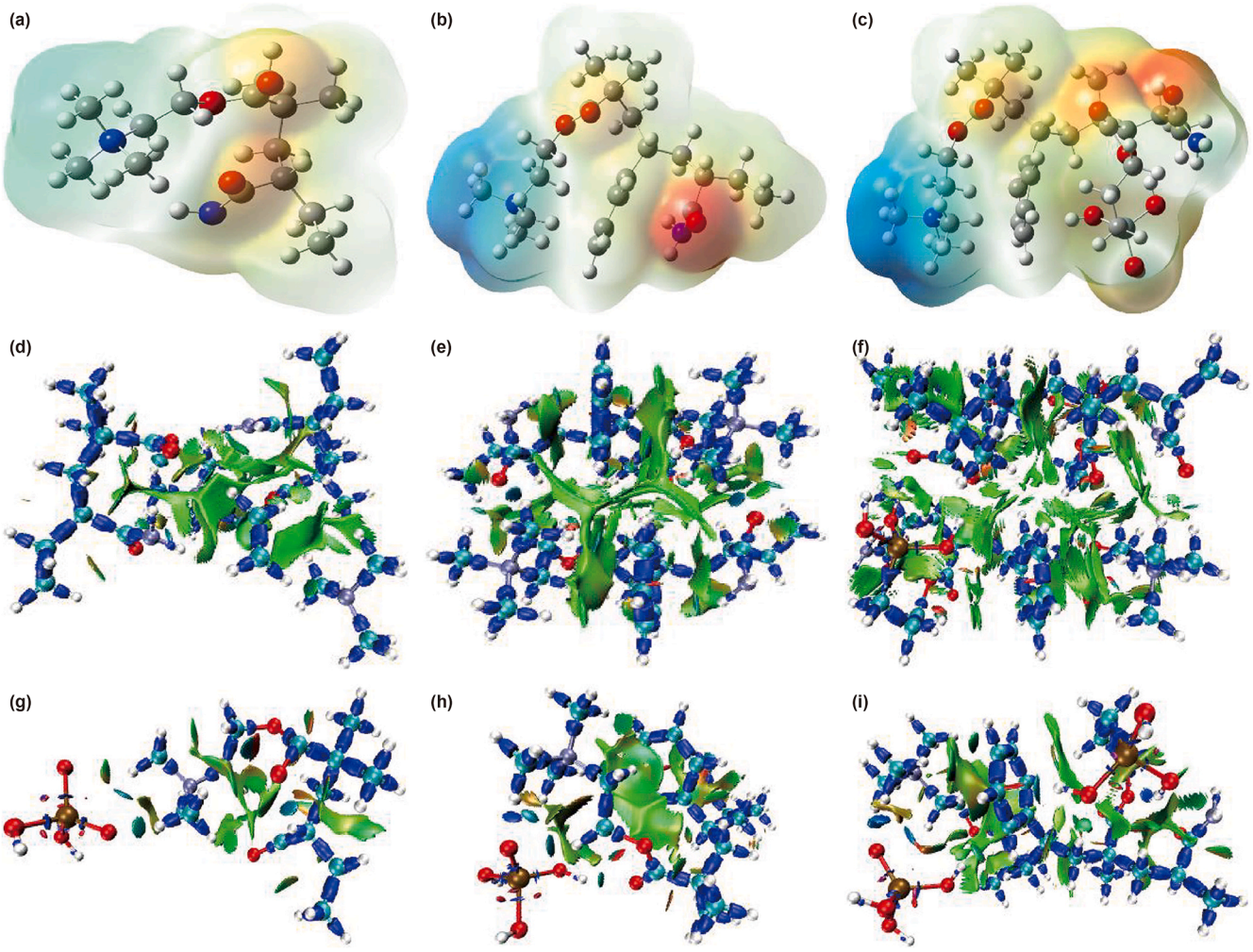

Fig. 13. Results of the theoretical simulations (DFT calculations). Top row: electrostatic potential maps of PDM (**a**), PDSM (**b**), and PDKM (**c**). Middle row: intermolecular interactions of PDM (**d**), PDSM (**e**), and PDKM (**f**). Bottom row: molecular interactions between sand grains and PDM (**g**), PDSM (**h**), and PDKM (**i**).

the interaction; the deeper the red color, the greater the steric hindrance; and the green color indicates weak interactions (Richardson, 2015; Lemos et al., 2024; Mouli et al., 2025). PDM–PDM, PDSM–PDSM, and PDKM–PDKM interactions are shown in Fig. 13(d)–(f), respectively. Similarly, Fig. 13(g)–(i) shows the interactions between quartz sand–PDM, quartz sand–PDSM, and quartz sand–PDKM, respectively.

The intermolecular IRI plots shown in Fig. 13(d)–(f) indicate that the blue IRI area in Fig. 13(f) is deeper than the blue areas in the PDM–PDM and PDSM–PDSM plots. This observation demonstrates the strongest intermolecular forces between two PDKM molecules, which is further supported by the calculated interaction energies. The interaction energy of PDKM (−0.065 Ha) is larger than both PDM (−0.044 Ha) and PDSM (−0.052 Ha). The results indicate that the intermolecular interactions between PDKM molecules, including π–π stacking, hydrogen bonding, and electrostatic attraction, are stronger than the other agents, leading to more stable and compact intermolecular network structures.

The interactions between agents and quartz sand are shown in Fig. 13(g)–(i). The IRI plots reveal that the sand–PDKM (Fig. 13(i)) has the most extensive blue interaction regions, indicating stronger binding of PDKM to the quartz surface compared to PDM (Fig. 13(g)) and PDSM (Fig. 13(h)). This observation is consistent with the calculated interaction energies: sand–PDM (−0.046 Ha), sand–PDSM (−0.070 Ha), sand–PDKM (−0.085 Ha). The strong electrostatic interaction between PDKM and quartz sand is attributed to strong hydrogen bonds. Note that the strongest electrostatic interaction is close to the strength of a chemical bond. Therefore, these strong interactions enable PDKM to adsorb more firmly onto the surface of quartz sand, providing a more effective adsorption and bridging effects that promote tighter aggregation of sand particles, thereby controlling their mobilization under fluid flow.

3.5.2. *Sand inhibiting and water control mechanisms*

The mechanisms of achieving simultaneous sand inhibiting and water control by PDKM are illustrated in Fig. 14. The parts labeled ‘A’ relate to sand inhibiting, and those labeled ‘B’ relate to water control.

3.5.2.1. Sand inhibiting mechanism. As shown in A1 (Fig. 14), PDKM molecules are strongly adsorbed onto the surface of quartz sand grains, forming a dense three-dimensional network structure (see Fig. 7). This network structure arises from intermolecular interactions of PDKM–PDKM and PDKM–sand, including electrostatic, π–π stacking, hydroxyl condensation, and hydrogen/hydroxyl bonding. An SEM image of intermolecular network structure formed by the PDKM is also shown in C, demonstrating

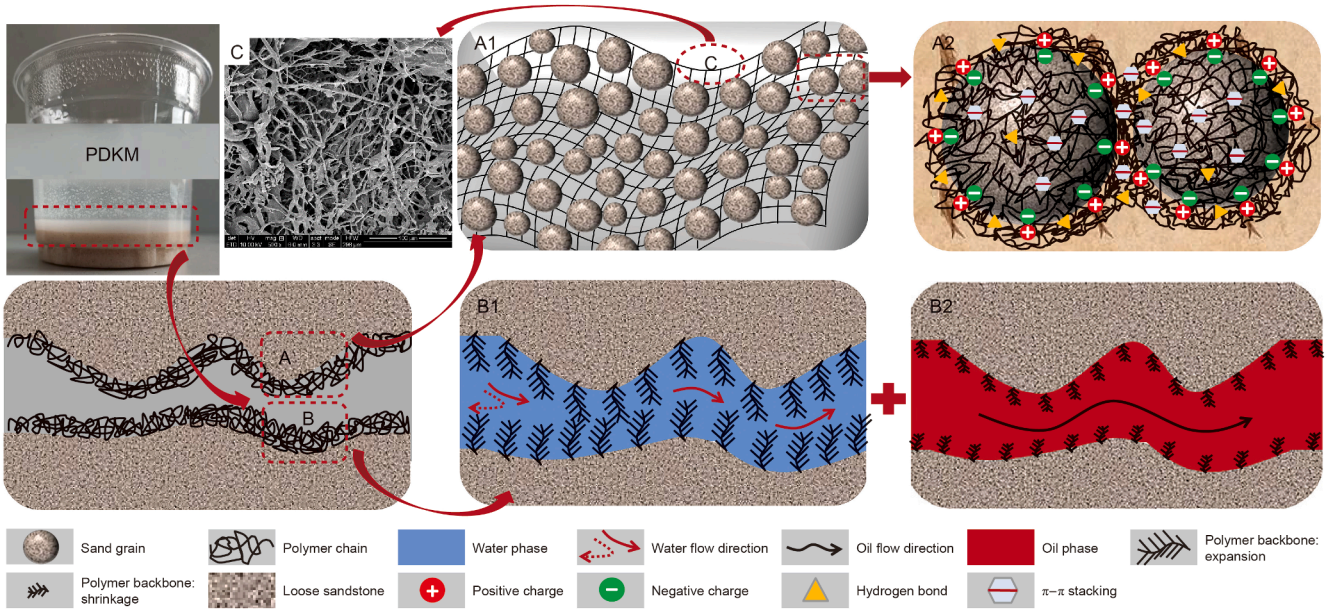

Fig. 14. Schematic diagrams of the mechanisms of achieving simultaneous sand inhibiting and water control by PDKM.

its "fishing net" configuration which serves as a protective net to prevent sand grain from detaching (see Fig. 10(a)). As shown in A2, two adjacent sand grains are firmly bridged (aggregated) by the intermolecular network structure of the agent (see Fig. 10(b)). Therefore, free individual sand grains are transformed into aggregates of multiple sand grains (see Fig. 10(c)), improving the overall stability of the sand grains and achieving desired sand inhibiting effect.

3.5.2.2. Water control mechanism. As shown in B (Fig. 14), PDKM molecules adsorbed onto the quartz sand surface form a polymer adsorption layer (or concentrate layer, see Fig. 10(a)) with selective water control effect through similar intermolecular interactions (electrostatic, π–π stacking, hydroxyl condensation, hydrogen/hydroxyl bonding). In B1, when the polymer adsorption layer encounters water, the polymer chains undergo hydration-induced swelling, adopting an anchor-shape structure that partially occludes pore throats. This effect significantly increases the flow frictional resistance of the water phase and reduces the permeability of the water layer (see Table 2). In B2, the polymer adsorption layer encounters oil, the polymer molecular chains shrink, increasing the effective aperture of the oil flow channel and significantly reducing the flow frictional resistance of the oil phase. Consequently, PDKM facilitates oil flow through the rock pores, indicating the permeability of the oil layer remains unaffected. Overall, this swelling–shrinking behavior results in flow control: hindering water phase flow while preserving or enhancing oil phase flow (see Table 2 and Fig. 12).

4. Conclusions

Building upon previous research, a novel supramolecular sand inhibiting and water control agent, PDKM, was successfully synthesized by incorporating the cationic monomers (DMC) and hydrophobic monomers (SM) into the polymer backbone, followed by the introduction of functional monomer KH570. KH570 can form hydrogen/hydroxyl bonds with quartz sand and enhance intermolecular interactions. The performance of PDKM was systematically compared with that of previously developed agents PDM and PDSM. The main conclusions are as follows:

(1) Benefiting from the synergistic effect of the three functional monomers DMC, SM, and KH570, PDKM exhibits a significantly lower sand production rate (0.02 g/L, which is 60.0% and 33.3% lower than that of PDM and PDSM, respectively) and a longer sand leakage time (665 s, which is 315.6% and 130.1% higher than PDM and PDSM, respectively). These results confirm that PDKM offers superior sand inhibiting/stabilization performance.

(2) Due to its denser intermolecular network structure and more pronounced macromolecular aggregation, PDKM establishes a higher standard water–oil resistance ratio (6.47, which is 98.5% and 15.5% higher than PDM and PDSM, respectively), and achieved a greater reduction in water cut (34.1%, which is 101.8% and 45.1% higher than PDM and PDSM, respectively). These observations demonstrate that PDKM has a more effective and selective water control effect.

(3) The theoretical simulations (DFT calculation) results further validate the experimental findings. Compared with PDM and PDSM, PDKM exhibits a stronger electrostatic potential (more concentrated positive charge), a higher intermolecular interaction energy (−0.065 Ha, which is 47.7% and 25.0% greater than PDM and PDSM, respectively), and a stronger adsorption onto quartz sand (−0.085 Ha, which is 84.8% and 21.4% greater in magnitude than PDM and PDSM, respectively). Therefore, compared to the PDM and PDSM, PDKM possesses stronger interactions with quartz sand and other PDKM molecules, better aggregating/bridging sand particles, and enhanced sand inhibiting and water control effects.

CRediT authorship contribution statement

Tian-Meng Lei: Writing – original draft, Methodology, Investigation, Formal analysis, Conceptualization. **Ye-Fei Wang:** Writing – review & editing. **Ming-Chen Ding:** Software, Project administration. **Wu-Hua Chen:** Software, Formal analysis. **Zhen-Ye Yu:** Software, Project administration. **Zhi-Xue Huang:** Formal analysis. **Motorova Kseniya Alexandrovna:** Visualization, Validation, Software, Resources.

Declaration of competing interest

The authors declare that they have no conflict of interest.

Acknowledgements

This work was supported by the National Natural Science Foundation of China (General Program, Grant No. 52474071) and the Provincial Key R&D Program of Shandong (2022CXGC020303). The authors gratefully acknowledge the financial support from the China Scholarship Council (T.-M. Lei, No. 202406450004).

References

Ahmed, A.A., Saaid, I.M., Shafian, S.R.M., 2020. Novel relative permeability modifier using polymer grafted nanoclay. Energy Fuels. 34 (3), 2703–2709. https://doi.org/10.1021/acs.energyfuels.9b03500.

Ahmed, A.A., Saaid, I.M., Sambo, C., et al., 2023. Experimental investigation and numerical simulation of relative permeability modifiers during water shut-off. Geoenergy Sci. Eng. 230 (12), 212095–212105. https://doi.org/10.1016/j.geoen.2023.212095.

Alakbari, F.S., Mohyaldinn, M., Muhsan, A.S., et al., 2020. Chemical sand consolidation: From polymers to nanoparticles. Polymers 12 (5), 1069–1099. https://doi.org/10.3390/polym12051069.

Askarinezhad, R., Hatzignatiou, D.G., Stavland, A., 2021. Associative polymers for disproportionate permeability reduction–formation wettability effects. J. Petrol. Sci. Eng. 206 (13), 109060–109074. https://doi.org/10.1016/j.petrol.2021.109060.

Chen, L.F., Huang, F.Y., Li, G., et al., 2023. Experimental study on fiber balls for bridging in fractured-vuggy reservoir. SPE J. 28 (4), 1880–1894. https://doi.org/10.2118/214315-PA.

Chen, L.F., Zhang, Z.N., Zeng, H.Y., et al., 2024. Preparation and performance of high-temperature-resistant, degradable inorganic gel for steam applications. SPE J. 29 (10), 4266–4281. https://doi.org/10.2118/219775-PA.

Deng, B., Jia, Z.W., Liu, W., et al., 2021. Selective water plugging technology for horizontal well with screen completion. Energies 14 (4), 791–805. https://doi.org/10.3390/en14040791.

Denney, D., 2001. Factors affecting mechanical water shutoff. J. Petrol. Technol. 53 (3), 58–59. https://doi.org/10.2118/0301-0058-JPT.

Duan, M., Wang, Q.H., Chen, B., et al., 2024. Preparation and performance evaluation of quaternary copolymer sand control agent. SPE J. 29 (5), 2288–2302. https://doi.org/10.2118/218415-PA.

Frisch, M.J., Trucks, G.W., Schlegel, H.B., et al., 2016. Application Program. Gaussian 16, Revision A.03. Wallingford CT.

Guo, A.J., Geng, Y.R., Zhao, L.L., et al., 2014. Preparation of cationic polyacrylamide microsphere emulsion and its performance for permeability reduction. Pet. Sci. 11 (5), 408–416. https://doi.org/10.1007/s12182-014-0355-0.

Hayavi, M.T., Kalantariasl, A., Malayer, M.R., 2023. Application of polymeric relative permeability modifiers for water control purposes: Opportunities and challenges. Geoenergy Sci. Eng. 231 (8), 212330–212369. https://doi.org/10.1016/j.geoen.2023.212330.

Humphrey, W., Dalke, A., Schulten, K., 1996. VMD: Visual molecular dynamics. J. Mol. Graph. 14 (1), 33–38. https://doi.org/10.1016/0263-7855(96)00018-5.

Huo, K.Y., Liu, W.J., Shou, Z.Y., et al., 2024. Modulating the interactions of peptide-polyphenol for supramolecular assembly coatings with controllable kinetics and multifunctionalities. Adv. Sci. 12 (3), 2412194–2412201. https://doi.org/10.1002/advs.202412194.

Joseph, J., Berville, M., Wytko, J., et al., 2024. π-mers and π-dimers: Two radical supramolecular interactions–A tutorial review. Chem. Eur. J. 31 (2), 1–12. https://doi.org/10.1002/chem.202403115.

Lai, N.J., Qin, X.P., Ye, Z.B., et al., 2013. The study on permeability reduction performance of a hyperbranched polymer in high permeability porous medium. J. Petrol. Sci. Eng. 112 (24), 198–205. https://doi.org/10.1016/j.petrol.2013.11.005.

Lei, T.M., Ding, M.C., Chen, W.H., et al., 2024. Preparation of novel polymeric surfactants based on synergistic effects and analysis of the mechanism driving the oil-displacement process and enhanced oil recovery. J. Mol. Liq. 415 (Part A), 126318–126330. https://doi.org/10.1016/j.molliq.2024.126318.

Lei, T.M., Wang, Y.F., Xue, X.F., et al., 2025. Preparation and performance evaluation of a novel sand–water dual-control functional polymer. Pet. Sci. 22 (2), 697–709. https://doi.org/10.1016/j.petsci.2024.10.008.

Lemos, R.P., Rodrigues, J.T., Portwood, G., et al., 2024. Evolution-based protein engineering: Functional switching between transthyretins and 5-hydroxyisourate hydrolases. J. Biomol. Struct. Dyn. 11 (20), 1–17. https://doi.org/10.1080/07391102.2024.2440647.

Li, J.D., Zhang, G.C., Ge, J.J., et al., 2022a. Self-aggregating behavior of poly(4-vinyl pyridine) and the potential in mitigating sand production based on π–π stacking interaction. Pet. Sci. 19 (5), 2165–2174. https://doi.org/10.1016/j.petsci.2022.06.001.

Li, J.D., Zhang, G.C., Ge, J.J., et al., 2022b. Self-healing elastomer modified proppants for proppant flowback control in hydraulic fracturing. Pet. Sci. 19 (1), 245–253. https://doi.org/10.1016/j.petsci.2021.12.025.

Li, L., Smitthipong, W., Zong, H.B., 2015a. Mussel-inspired hydrogels for biomedical and environmental applications. Polym. Chem. 6 (3), 353–358. https://doi.org/10.1039/C4PY01415D.

Li, L., Yan, B., Yang, J.Q., et al., 2015b. Novel mussel-inspired injectable self-healing hydrogel with anti-biofouling property. Adv. Mater. 27 (7), 1294–1299. https://doi.org/10.1002/adma.201405166.

Li, L., Yan, B., Zhang, L., et al., 2015c. Mussel-inspired antifouling coatings bearing polymer loops. Chem. Commun. 51 (87), 15780–15784. https://doi.org/10.1039/c5cc06852e.

Li, L., Liu, J.W., Chen, J., et al., 2022. Mussel-inspired hydrogel particles with selective adhesion characteristics for applications in reservoir fracture control. J. Mol. Liq. 361 (9), 119598–119606. https://doi.org/10.1016/j.molliq.2022.119598.

Li, L., Dong, Y.B., Jin, X., et al., 2024. A cationic type long-lasting drag-reduction agent based on reduced interfacial water film thickness for enhanced injection in low-permeability reservoirs. J. Mol. Liq. 398 (15), 124294–124304. https://doi.org/10.1016/j.molliq.2024.124294.

Li, X.Q., Zhang, G.C., Ge, J.J., et al., 2017. Organosilane film for sand migration control based on in-situ hydrolysis and polycondensation effects. J. Petrol. Sci. Eng. 158 (17), 660–671. https://doi.org/10.1016/j.petrol.2017.08.013.

Li, Y.K., Li, Y.X., Peng, Y., et al., 2019. Water shutoff and profile control in China over 60 years. Oil Drilling & Production Technology 41 (6), 773–787 (in Chinese).

Lu, T., Chen, Q.X., 2021. Interaction region indicator (IRI): A simple real space function clearly revealing both chemical bonds and weak interactions. Chem. Mater. 1 (5), 231–239. https://doi.org/10.26434/chemrxiv.13591142.

Luo, Q., Tang, K., Bai, L., et al., 2022. Development of in-situ starch grafted copolymerized gels for conglomerate reservoir conformance control and oil recovery improvement. J. Petrol. Sci. Eng. 210 (9), 110005–1100016. https://doi.org/10.1016/j.petrol.2021.110005.

Marandi, S.Z., Salehi, M.B., Moghadam, A.M., et al., 2018. Sand control: Experimental performance of polyacrylamide hydrogels. J. Petrol. Sci. Eng. 170 (32), 430–439. https://doi.org/10.1016/j.petrol.2018.06.074.

Mouli, H.M.C., Harini, D., Shaikh, N., et al., 2025. In silico characterization of indole-substituted densely functionalized pyrrole against breast cancer: Integrating DFT, molecular docking, MD simulations, and ADME analysis. J. Mol. Struct. 1328 (11), 141375–141388. https://doi.org/10.1016/j.molstruc.2025.141375.

Niu, W.J., Nie, W., Bao, Q., et al., 2025. Molecular mechanisms of coal dust wettability: Hydrophilic group modulation for enhanced surface interactions. Appl. Surf. Sci. 686 (30), 162146–162158. https://doi.org/10.1016/j.apsusc.2024.162146.

Qi, Z.H., Wang, Y.F., Liu, C., et al., 2013. A laboratory evaluation of a relative permeability modifier for water production control. Petrol. Sci. Technol. 31 (22), 2357–2363. https://doi.org/10.1080/10916466.2011.592892.

Qiao, R., Zhu, W.Q., 2010. Evaluation of modified cationic starch for impeding polymer channeling and in-depth profile control after polymer flooding. J. Ind. Eng. Chem. 16 (2), 278–282. https://doi.org/10.1016/j.jiec.2009.09.070.

Qin, L.M., Arjomand, E., Myers, M.B., et al., 2020. Mechanistic aspects of polymeric relative permeability modifier adsorption onto carbonate rocks. Energy Fuels. 34 (10), 12065–12077. https://doi.org/10.1021/acs.energyfuels.0c01590.

Richardson, S.J., 2015. Tweaking the structure to radically change the function: The evolution of transthyretin from 5-hydroxyisourate hydrolase to triiodothyronine distributor to thyroxine distributor. Front. Endocrinol. 5 (11), 245–254. https://doi.org/10.3389/fendo.2014.00245.

Rijns, L., Rutten, M., Bellan, R., et al., 2024. Synthetic, multi-dynamic hydrogels by uniting stress-stiffening and supramolecular polymers. Sci. Adv. 10 (47), 3209–3226. https://doi.org/10.1126/sciadv.adr3209.

Ross, C.M., Rangel-German, E.R., Castanier, L.M., et al., 2006. A laboratory investigation of temperature-induced sand consolidation. SPE J. 11 (52), 206–215. https://doi.org/10.2118/92398-MS.

Salehi, M.B., Moghadam, A.M., Marandi, S.Z., 2019. Polyacrylamide hydrogel application in sand control with compressive strength testing. Pet. Sci. 16 (4), 94–104. https://doi.org/10.1007/s12182-018-0255-9.

Semichem, Inc., 2019. Application Program. Gaussview, Version 6.0.16.

Seright, R., Brattekas, B., 2021. Water shutoff and conformance improvement: An introduction. Pet. Sci. 18 (35), 450–478. https://doi.org/10.1007/s12182-021-00546-1.

Shu, Z., Qi, Y., Luo, P.Y., 2023. Research and performance evaluation of modified nano-silica gel plugging agent. J. Appl. Polym. Sci. 140 (21), 53873–53889. https://doi.org/10.1002/app.53873.

Sun, X.D., Bai, B.J., 2017. Comprehensive review of water shutoff methods for horizontal wells. Petrol. Explor. Dev. 44 (6), 967–973. https://doi.org/10.11698/PED.2017.06.15.

Tang, C.Y., Li, Y., Fei, X., et al., 2024. An integrally formed Janus supramolecular biogel with intelligent adhesion for multifunctional healthcare. J. Colloid Interface Sci. 680 (Part A), 1030–1041. https://doi.org/10.1016/j.jcis.2024.11.056.

Tian, K.P., Pu, W.F., Zhao, S., 2023. Synthesis of high strength agar and its water plugging application in enhanced oil recovery. Petrol. Sci. Technol. 42 (20), 2705–2724. https://doi.org/10.1080/10916466.2023.2175863.

Wu, Y.H., Duan, M., Wang, Q.H., et al., 2024. Dispersion polymerization of AM-AMPS-DAM-DOH and its sand control property. Geoenergy Sci. Eng. 241 (5), 213190–213199. https://doi.org/10.1016/j.geoen.2024.213190.

Xu, Z., Sun, J.S., Liu, J.P., et al., 2024. Development and performance evaluation of high temperature resistant strong adsorption rigid blocking agent. Pet. Sci. 21 (4), 2650–2662. https://doi.org/10.1016/j.petsci.2024.03.021.

Ye, Z.B., He, E.Q., Xie, S.Y., et al., 2010. The mechanism study of disproportionate permeability reduction by hydrophobically associating water-soluble polymer gel. J. Petrol. Sci. Eng. 72 (1–2), 64–66. https://doi.org/10.1016/j.petrol.2010.03.004.

Zhang, C., Zhou, Z.Y., Xi, M.N., et al., 2025. Molecular modeling to elucidate the dynamic interaction process and aggregation mechanism between natural organic matters and nanoplastics. Eco-Environ. Health 4 (1), 100122–100131. https://doi.org/10.1016/j.eehl.2024.08.004.

Zhu, D., Peng, S., Zhao, S., et al., 2021. Comprehensive review of sealant materials for leakage remediation technology in geological CO_2 capture and storage process. Energy Fuels. 35 (6), 4711–4742. https://doi.org/10.1021/acs.energyfuels.0c04416.